Solar Physics (2021) 296:160
https://doi.org/10.1007/s11207-021-01902-5

Solar Event Detection Using Deep-Learning-Based Object Detection Methods

Ji-Hye Baek[1,2,3] · Sujin Kim[2] · Seonghwan Choi[1,2] · Jongyeob Park[1,2] · Jihun Kim[1,2] · Wonkeun Jo[3] · Dongil Kim[3]

Received: 18 May 2021 / Accepted: 18 September 2021 / Published online: 8 November 2021

Abstract
Research on the detection of solar events has been conducted over many years. Recently, deep learning and data-driven approaches have been applied to solar event recognition. In this study, we present solar event detection using deep-learning-based object detection methods for real-time space weather monitoring. First, we construct a new object detection dataset using imaging data obtained by the Solar Dynamics Observatory with bounding boxes as labels for three representative features: coronal holes, sunspots, and prominences. Second, we train two representative object detection models: the Single Shot MultiBox Detector (SSD) and the Faster Region-based Convolutional Neural Network (R-CNN) using the new dataset. The results show that both models perform similarly well for coronal hole and sunspot detection. For prominence detection, the SSD and Faster R-CNN exhibited relatively low performance. This study demonstrates that deep-learning-based object detection can successfully detect multiple types of solar events, and it may be extended to detect other solar events. In addition, we provide the dataset for further achievements of object detection studies in solar physics.

Keywords Event detection · Data management · Sunspots · Coronal holes · Prominences

1. Introduction

In the field of solar physics, feature detection on the surface of the Sun is an important topic. Solar event detection using images is primarily based on conventional image processing

✉ D. Kim
dkim@cnu.ac.kr

J.-H. Baek
jhbaek@kasi.re.kr

1 Technology Center for Astronomy and Space Science, Korea Astronomy and Space Science Institute, 776 Deadeok-daero, Yuseong-gu, Daejeon 34055, Republic of Korea

2 Space Science Division, Korea Astronomy and Space Science Institute, 776 Deadeok-daero, Yuseong-gu, Daejeon 34055, Republic of Korea

3 Department of Computer Science and Engineering, Chungnam National University, 99 Daehak-ro, Yuseong-gu, Daejeon 34134, Republic of Korea

algorithms and neural network learning algorithms which apply the artificial intelligence technology. The solar phenomena observed in the solar atmosphere include sunspots, filaments, coronal holes, prominences, coronal loops, active regions, and sigmoids. Because the characteristics of solar events are different, a feature detection algorithm that is optimized for the characteristics of each event is necessary. Aschwanden (2010) introduced four image analysis methods for solar event feature detection: curvilinear one-dimensional (1D), region-based (2D), spectral methods, and artificial intelligence. Curvilinear 1D feature detection is used to extract the features of loops and images by applying a high-pass filter (Lee, Newmann, and Gary, 2006; Aschwanden et al., 2008; Inhester, Feng, and Wiegelmann, 2008). Region-based (2D) feature detection is used to determine approximate outlines of solar events, such as sunspots, active regions, and filaments. Additionally, the following conventional computer vision methods are applied: labeling, symmetrical difference, dilation, erosion, morphological gradient distance transform, opening, closing, conditional dilation, closed holes, hit-or-miss transform, thinning, thickening, skeleton pruning, watershed (McAteer et al., 2005; Curto, Blanca, and Martinez, 2008; Martens et al., 2012). The spectral method decomposes spatial images into spatial Fourier components in the form of a power spectrum. This method is similar to the Fourier or wavelet analysis of time-series data, and it is used to detect active regions and filaments (Ireland et al., 2008; Portier-Fozzani et al., 2001). A neural network, which is an artificial intelligence approach, is applied after undergoing a learning process using data. It is primarily applied to classification, and it can be used in any of the three above mentioned methods (Banda and Angryk, 2010, 2014).

Detection refers to the accurate identification of an object area, which is a basic problem in computer vision. Object recognition is a combination of object localization and image classification; therefore, it is a more difficult and complex problem compared with image classification. Various algorithms for object detection have been proposed, and the detection of the area of an object determines the accuracy and speed of the model (Huang et al., 2017). The object detection algorithm extracts features from an object to be searched; it then detects the features in the image and classifies them using these features. Many object detection models based on deep learning and convolutional neural networks (CNNs) have been proposed in recent studies. Both the Single Shot MultiBox Detector (SSD) (Liu et al., 2016) and "You Only Look Once" (YOLO) (Redmon et al., 2016) systems process classification and localization simultaneously; these are called 1-stage detectors. YOLO defines the object detection problem as a regression and obtains the bounding box coordinates and class probability directly from the input image. However, YOLO uses a single-scale feature map, whereas SSD extracts features using multi-scale feature maps. Thus, SSD is faster and more accurate than YOLO (Liu et al., 2016). Region-based CNN series models (R-CNN (Girshick et al., 2014), Fast R-CNN (Girshick, 2015), Faster R-CNN (Ren et al., 2017), Mask R-CNN (He et al., 2017), Cascade R-CNN (Cai and Vasconcelos, 2018), and Region-based Fully Convolutional Networks (R-FCN) (Dai et al., 2016), known as 2-stage detectors, perform localization and classification in sequence. R-CNN solves the CNN localization problem by applying recognition using the region paradigm. The R-CNN model extracts objects from proposed regions and trains them individually through classification and box regression. Owing to such a complex process, the optimization of this method is limited; R-CNN also has the disadvantage of a large inference time. To improve R-CNN, state-of-the-art object detection systems have been proposed, such as Fast R-CNN, Faster R-CNN, R-FCN, Mask R-CNN, and Cascade R-CNN.

Current advances in object detection based on deep learning have enabled the expansion of practical object identification in various fields, such as medical imaging, geography, and geology. Solar phenomena detection has been attempted in the field of solar physics.

Kucuk, Banda, and Angryk (2017) studied the classification of solar events, such as active regions, coronal holes, flares, sigmoids, and quiet-Sun regions using deep CNN models, and they showed that the accuracy of deep learning CNNs was significantly higher than that of conventional classification methods. Kucuk, Aydin, and Angryk (2017) detected active regions and coronal holes in multi-wavelength solar images from the Solar Dynamics Observatory (SDO) using Faster R-CNN, and they showed that supervised deep-learning-based object detection can be applied to the solar physics domain. Moreover, Armstrong and Fletcher (2019) classified filaments, flare ribbons, prominences, sunspots, and quiet-Sun regions using a deep CNN. They showed that a deep learning model, trained using Hinode/Solar Optical Telescope data, can classify unseen images from the SDO/Atmospheric Imaging Assembly (AIA).

In this study, we focus on detecting three types of solar events (sunspots, prominences, and coronal holes) from three different wavelength datasets obtained by the SDO. We present solar event detection using SSD and Faster R-CNN, which are representative object detection systems, and compare the results between them. The novelty of this study is as follows:

- Unlike previous studies (Kucuk, Aydin, and Angryk, 2017; Kucuk, Banda, and Angryk, 2017), we created our own datasets for training and testing using SDO data. SDO is one of the largest real solar image repositories. However, because there is no label for each solar event and its location, deep learning methods have rarely been employed. We employ two subject experts to assign labels to each image to create a dataset that is appropriate for deep learning, which has not been attempted in the field of solar physics.
- Solar event detection using deep learning methods has been attempted. However, previous studies trained classification models using cropped images (Kucuk, Banda, and Angryk, 2017; Armstrong and Fletcher, 2019), which output only the image class, but not the location of the event. Kucuk, Aydin, and Angryk (2017) employed object detection methods; however, the accuracy of these methods was relatively low. We utilize more diverse solar events (coronal holes, sunspots, and prominences) and advanced object detection algorithms (SSD and Faster R-CNN). We achieve a more accurate model using object detection approaches that output both the solar event and its location. Additionally, our model is capable of classifying events in a relevant area in a solar full-disk image.

The remainder of this paper is organized as follows. Section 2 provides background information on solar events, SDO, and deep-learning-based object detection algorithms. In Section 3, we present our methodology, including the data preparation and object detection algorithms that we use. In Section 4, we present our experiments and results. Finally, in Section 5, we conclude the article with an outline of our future work.

2. Background

2.1. Solar Events

The Sun is a dynamic star, which is the energy source for the Earth and the entire heliosphere. Representative solar phenomena include sunspots, flares, prominences, and coronal holes (Kim, Park, and Kim, 2017; Brajša et al., 2018). A sunspot is a dark area that has strong magnetic energy in the photosphere; associated loops appear bright in the upper atmosphere, chromosphere, and corona (Priest, 2014). A flare is an energy release event that occurs in

an active region which usually contains sunspots; it produces a strong emission at all wavelengths. Thus, sunspots are classified as active regions (ARs) with AR numbers assigned by the National Oceanic and Atmospheric Administration. A prominence is a chromospheric cool plasma structure held by the magnetic filed in the corona; it appears as a dark and thin "filament" on the solar disk or as a bright "prominence" in the off-limb region. When it becomes unstable, its large mass is expelled as a coronal mass ejection into the interplanetary space. A coronal hole, which is the source of high-speed solar wind, is observed as a quiet dark hole in the corona. Because these phenomena are key factors that affect space weather, it is important to detect and monitor them consistently.

2.2. Solar Dynamics Observatory (SDO)

SDO is designed to understand the Sun and the effect of solar activity on Earth. SDO has the following scientific instruments: the AIA, the Helioseismic and Magnetic Imager (HMI), and the Extreme Ultraviolet (EUV) Variability Experiment (EVE). AIA observes the solar atmosphere using multiple channels with 10 wavelengths (94, 131, 171, 193, 211, 304, 335, 1600, 1700, and 4500 Å) every 12 seconds (Lemen et al., 2012). HMI explores the Sun's interior and magnetic fields using magnetogram and intensitygram with temporal cadences of 45 seconds and 720 seconds (Schou et al., 2012). EVE aims to probe the changes in the Sun's ultraviolet irradiance and magnetic fields, and it produces solar EUV data of 0.1 – 105 nm with a spectral resolution of 0.1 nm and a 10-second temporal cadence (Woods et al., 2012).

AIA and HMI produce high-resolution 4096 × 4096 pixel images and generate 1.5 TB of data every day since 2010. The total data size from SDO to date is approximately 5 PB. This big data set obtained by SDO enables various studies and the application of deep learning techniques in solar physics (Armstrong and Fletcher, 2019; Jeong et al., 2020; Kim et al., 2019; Kucuk, Aydin, and Angryk, 2017; Park et al., 2018, 2020; Rahman et al., 2020). We use SDO/AIA and HMI data to train the solar event auto-detection models.

2.3. Object Detection Algorithms

Object recognition is a computer vision technology that identifies specific object instances in an image or video. Recent advancements in object detection methods include CNN and deep learning. Various deep-learning-based models have been proposed, such as YOLO, SSD, RetinaNet (Lin et al., 2017), RefineDet (Zhang et al., 2018), R-CNN family (R-CNN, Fast R-CNN, Faster R-CNN, Mask R-CNN, and Cascade R-CNN), and R-FCN.

YOLO processes feature extraction, bounding box, and classification simultaneously through unified detection. The unified detection combines parts of the divided detection model into a single neural network and enables high-speed processing with high accuracy (Redmon et al., 2016). However, YOLO cannot detect objects that are smaller than the grid size, and it can only detect one object per grid cell because it divides a predetermined grid and performs a bounding box prediction. SSD is a technique that detects objects in images using a single deep neural network. SSD is faster and more accurate than YOLO, and it has a higher accuracy than other techniques, such as Faster R-CNN that uses region proposal and pooling (Liu et al., 2016). SSD creates several default boxes with different aspect ratios and scales in a feature map. When making predictions, each default box is scored for the object category and adjusted to a box that matches the object shape. SSD is relatively simpler than methods that require region proposals because the proposal generation and subsequent pixels completely eliminate the feature resampling stage; thus all computational processes are summarized in one network. In general, since the number of objects in an image is small,

less areas are predicted for positive samples (objects) than negative samples (background). To solve such class imbalances, RetinaNet proposes a new function termed the focal loss and improves its performance (Lin et al., 2017). RefineDet proposes a 1-stage detector that has the advantages of 2-stage detectors (less class imbalances and more sophisticated predictions due to the use of a two-step cascade with two-step features) by adding the anchor refinement module (ARM), object detection module (ODM), and transfer connection block (TCB) (Zhang et al., 2018).

R-CNN suggests a region-based convolutional neural network. The features are extracted by passing 2000 region proposals, which are obtained using a selective search and deep CNN, and the regions are classified based on the features. R-CNN improves the performance of object detection (Girshick et al., 2014). However, R-CNN is slow because 2000 region proposals must be processed in a deep CNN forward pass for each object proposal. Fast R-CNN was proposed to improve the test-time speed. Instead of putting each region proposal into a CNN, the entire image was placed directly into the CNN to create a feature map, thereby reducing the training and testing speed of the model and improving performance (Girshick, 2015). However, Fast R-CNN is still slow in terms of processing region proposals based on a selective search. Faster R-CNN introduces the Selective Search Region Proposal Network, which is a method that calculates region proposals using a deep network. Faster R-CNN reduces the learning time by sharing the detection network and convolutional layer for region proposals (Ren et al., 2017). Mask R-CNN detects more specific object (instance) areas by adding a region of interest (RoI) to generate segmentation masks for the detection boxes from Faster R-CNN and to even estimate human poses (He et al., 2017). Cascade R-CNN proposes a method of maximizing the model by learning with a higher intersection-over-union (IoU) criterion (greater than 0.8) using additional classifiers (Cai and Vasconcelos, 2018), whereas Faster R-CNN uses a single classifier.

3. Proposed Methods

3.1. Data

We coupled coronal holes, sunspots, and prominences as solar events for the detection experiment. These events were selected as relatively recognizable phenomena in the Sun and were extracted clearly using the wavelengths of the SDO/AIA and HMI. Each coronal hole, sunspot, and prominence could be recognized on AIA 193, HMI intensitygram, and AIA 304, respectively (Lemen et al., 2012; Scherrer et al., 2012). We used full-disk SDO data from the Korean Data Center for SDO (`http://sdo.kasi.re.kr`) spanning ten years from 2010 to 2019. The data were sampled at 12-hour intervals for sunspots and coronal holes, and at 4-hour intervals for prominences. Original SDO images are in the FITS format (4096×4096 pixels). Because the events we wanted to extract were also visible even in lower-resolution images, we used the JPEG format (512×512 pixels). Samples of each solar event with bounding boxes and labeling are shown in Figure 1.

Object detection requires supervised learning; therefore, image label data is also required for training. Event catalogues and label data for deep learning are completely different. Event catalogues contain the position of the center at the event location, whereas label data include bounding boxes (event area) where the event is located. Besides, there is no public event label dataset. In previous solar event detection and classification studies that used deep learning algorithms (Kucuk, Aydin, and Angryk, 2017; Kucuk, Banda, and Angryk, 2017),

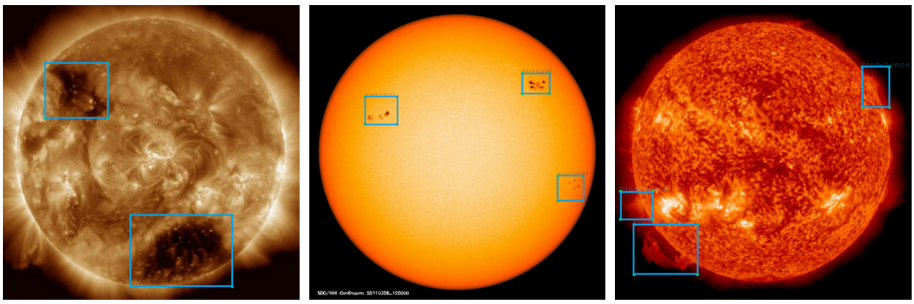

Figure 1 Examples of the application of bounding boxes and event labeling on the SDO data. Coronal hole instances on AIA 193 (left), sunspot instances on the HMI intensitygram (middle), and prominence instances on AIA 304 (right).

Table 1 Number of images for solar event detection.

Solar Events	Coronal hole	Sunspot	Prominence
SDO Instrument	AIA 193	HMI Intensitygram	AIA 304
Number of images	5085	4383	2926
Training set	4068	3500	2340
Test set	1017	883	586

the input dataset was the event list used in conventional image processing methods. Kucuk, Banda, and Angryk (2017) used the Large-Scale Solar Dynamics Observatory Dataset (LSDO), and Kucuk, Aydin, and Angryk (2017) used the Heliophysics Event Knowledgebase (HEK) (Hurlburt et al., 2012) for solar event reports. However, they did not publish their label datasets.

Since there is no label dataset for solar events, we created our own dataset. We used an image annotation and labeling tool called LabellImg (Tzutalin, 2015). LabelImg has capabilities to create data that includes the position of the bounding box and labeling information by drawing a box around the object that the user wants to find in the image and then labels the object. Solar physics experts identified the events, drew bounding boxes, and labeled them on the images using LabelImg. We defined the events which had clearly visible features, and drew the bounding box around each event. In the case of sunspots, we made a single box not only for a sunspot but also for sunspot groups that were relatively close to other. Two experts performed cross-validations to increase the event annotation and labeling accuracy of the entire dataset. The saved file format for the bounding box and labeling information of LabelImg can be Pattern Analysis, Statistical Modelling, and Computational Learning (PASCAL)/Visual Object Classes (VOC) in the Extensible Markup Language (XML) format or YOLO in text format; we used the PASCAL/VOC type. After this process, the input dataset of the object detection models included solar images and XML files with the bounding box position and labeling information. The number of data points used for solar event detection was 5085, 4383, and 2926 for coronal holes, sunspots, and prominences, respectively. The ratio of the training data to the test (unseen) data was 80:20. Table 1 shows the number of images used for the solar event detection with the number of event labels contained in the dataset for each event type.

Table 2 Number of solar events for our dataset and HEK dataset.

	Coronal hole	Sunspot	Prominence	Total
Our dataset	9984	11244	9241	30469
HEK dataset	7198	8857	82	16137

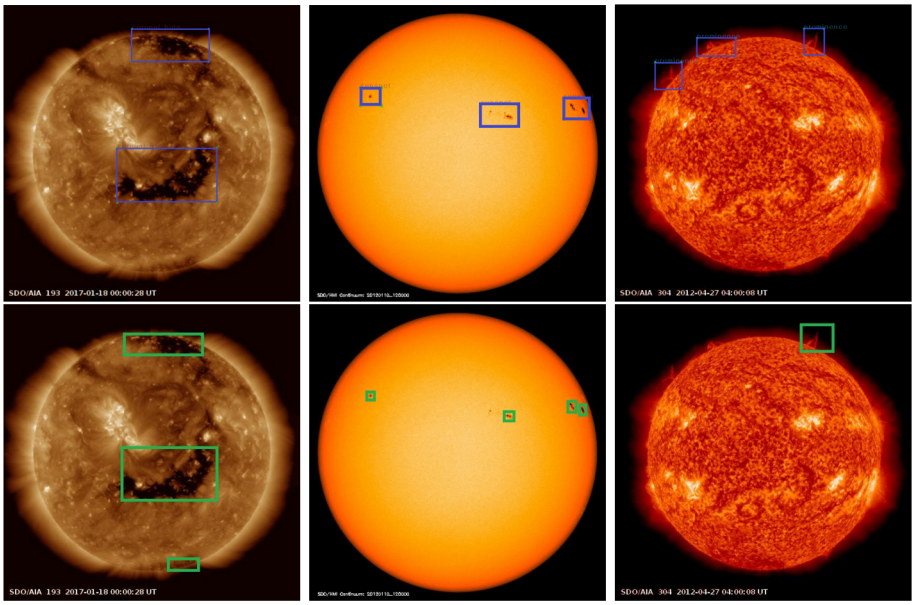

Figure 2 The event bounding boxes of our dataset (top) and HEK dataset (bottom). The left column shows coronal holes, the middle column shows sunspots, and the right column shows prominences.

We compared our dataset to the HEK data to prove its reliability and to compare targets with the number of events and bounding boxes. We matched bounding boxes based on event positions and classes labeled as event types in the HEK dataset. The event types in the HEK dataset included coronal holes and sunspots, but prominences did not exist separately but were included in the filament database. Thus, we extracted prominences that could be clearly identified based on the event description of the filament database in the HEK dataset. We compared events of our dataset and the HEK dataset during the target period (from 2010 to 2019). Table 2 shows the number of each event type in our dataset and the HEK dataset. The numbers of total events were 30,469 for our dataset and 16,137 for the HEK dataset. In our dataset, the number of events was evenly distributed. Whereas, in the HEK dataset, the number of coronal holes and sunspots were similar to each other; however, the number of prominences was 82, which was less than 1% of the entire dataset.

We drew by eye bounding boxes for each event to compare event locations between both datasets. In the case of coronal holes, event locations of our dataset and the HEK dataset were similar to each other. In the case of sunspots, our dataset considered the boundary of the entire area of the sunspot group, whereas the HEK dataset selected only relatively large sunspots in most cases. In the case of prominences, many of prominences in our dataset were not listed in the HEK dataset. Figure 2 shows the examples of bounding boxes for

our dataset (top) and HEK dataset (bottom). In the case of coronal holes (left column), the area and position of coronal holes in the north pole and central disk were well matched in both datasets while the small coronal hole near the south pole was only included in the HEK dataset. In the case of sunspots (middle column), our dataset considered a region that included a sunspot group, whereas the HEK dataset included only a small area with relatively large sunspots. This was the reason why the sunspot numbers of the HEK dataset were less than those of our dataset. In the case of prominences (right column), our dataset specified three prominences in the north limb, whereas the HEK dataset had only one.

As a result of comparison of our dataset and the HEK dataset, we found that the size and location of the bounding boxes were similar only in the case of the coronal holes. In the case of sunspots, the detection results of HEK and our dataset were different, probably owing to the difference in the detection criteria of events. For object detection, a well-defined dataset with bounding boxes that sufficiently cover the area of the object to be found is important. Since the HEK dataset was not constructed for deep-learning-based object detection, the bonding boxes did not seem suitable as labels. As shown in Figure 2, we provided better bounding boxes for the object detection, which implied that our dataset[1] is suitable for training deep learning models that automatically detect solar events.

3.2. Model Configuration

We selected representative object detection models, namely SSD as a 1-stage detector and Faster R-CNN as a 2-stage detector. Since the introduction of these two models, many models such as Mask R-CNN, RetinaNet, RefineDet, and Cascade R-CNN have been proposed. However, the basic structures of these models are similar to those of the SSD or Faster R-CNN. RefineDet is one of the SSD-series models with additional modules. Mask R-CNN and Cascade R-CNN add new layers to Faster R-CNN to predict a new parameter or to improve the performance. The use of these models has no significant advantage for detecting solar events; thus, we chose the SSD and Faster R-CNN.

We used SSD and Faster R-CNN architectures with ResNet-101 as the feature extractor provided by the TensorFlow object detection API. The accuracy and speed of the object detector vary depending on the feature extractor (Huang et al., 2017). The feature extractor has a key influence on the number of parameters or the types of layers, and these directly affect the memory usage, speed, and performance of the detectors. We selected ResNet-101 because it configures an appropriate combination that considers the optimal accuracy, memory usage, and training time ratio (Huang et al., 2017). ResNet solves gradient vanishing using shortcut connections, and improves the performance of deep CNNs (He et al., 2016).

TensorFlow provides pretrained models of an object detection application programming interface (API) using Common objects in Context (COCO) and ImageNet. However, real-life images from COCO and ImageNet are completely different from those of the Sun and solar events. There is no advantage from using pretrained codes with COCO and ImageNet; therefore, we trained models using the solar event dataset that we developed. We set the image sizes to 512 $\times$ 512 pixels and the batch size to 24 for the two models. For SSD, we set the activation function as RELU, the loss function as a sigmoid, and the initial learning rate to 0.002. For Faster R-CNN, the number of region proposals should be set manually. Usually, Faster R-CNN uses 300 region proposals. However, as shown in Huang et al. (2017), the accuracy of Faster R-CNN using only 50 region proposals resulted in

[1] Our dataset is available online on http://sdo.kasi.re.kr/dataset_object_detection.aspx.

Table 3 Summary of the performance of SSD and Faster R-CNN for the mAPs and detection accuracy of solar events.

Model	mAP (@0.5IoU[a])	Accuracy [%]		
		Coronal hole	Sunspot	Prominence
SSD	82	77	79	51
Faster R-CNN	79	76	80	45

[a]The ratio of IoU between predicted and ground truth boxes is greater than 0.5.

96% of that of the model using 300 region proposals. Moreover, increasing the number of proposed regions from 300 to 600 did not significantly affect the accuracy (Kucuk, Aydin, and Angryk, 2017). Therefore, we reduced the number of region proposals to 50. Additionally, we set the score converter at the second stage as softmax and the initial learning rate to 0.0002.

4. Experimental Results

The trained object detection models were from the deep learning framework TensorFlow. The models were trained on a GPU server dedicated to deep learning using four NVIDIA TITAN XP 12 GB GPUs. For training and testing, we used 10-year data from 2010 to 2019 and divided the training and evaluation data in the ratio of 80% and 20%, respectively. We selected two object detection models, namely Faster R-CNN and SSD, for solar event detection and compared the results of these two models.

We used the accuracy, average precision (AP), mean average precision (mAP), and true positive rates (TPRs) to evaluate the performance of the two models. In the field of computer vision, the performance of object detection and image classification algorithms is evaluated using AP. In the case of multiple object classes, the performance of the algorithm is evaluated using mAP, which is calculated using the AP for each class. The TPR (i.e. recall) is the proportion of correctly detected objects. To increase the TPR, the model must specify many bounding boxes to correct the answer and reduce the false negative (FN) detections. We used a cut-off point for the correctness criterion of the measurements. The detection results are considered correct if the intersection over union (IoU) (based on the Jaccard overlap) between the bounding boxes of our dataset and predicted boxes is greater than 0.5. Among the regions predicted by the models, we also used prediction boxes with a detection score of 0.8, or higher, when calculating the AP and TPR.

The performance of the two models is presented in Table 3. Our results for the detection accuracy based on mAP (@0.5IoU) are 82% and 79% for SSD and Faster R-CNN, respectively. The detection accuracies for different solar events are similar for SSD and Faster R-CNN, except for prominence detection. The prominence detection has a lower accuracy than the other events for both models; the accuracy is less than 50% using Faster R-CNN.

For further inspection of the trained models, we analyzed the AP and TPR scores. Figure 3 shows the AP of the models for each solar event. A higher AP indicates that the events are classified more precisely. The AP of coronal holes and sunspots using SSD and Faster R-CNN was higher than 90%. The highest AP was 99% for sunspot detection using SSD, which is considered a remarkable performance. For prominence detection, the APs

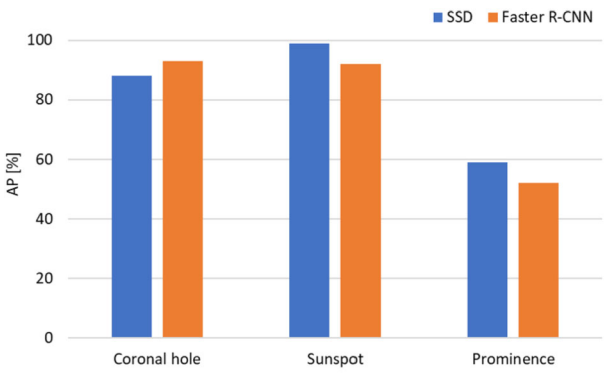

Figure 3 AP of the trained models for different solar events.

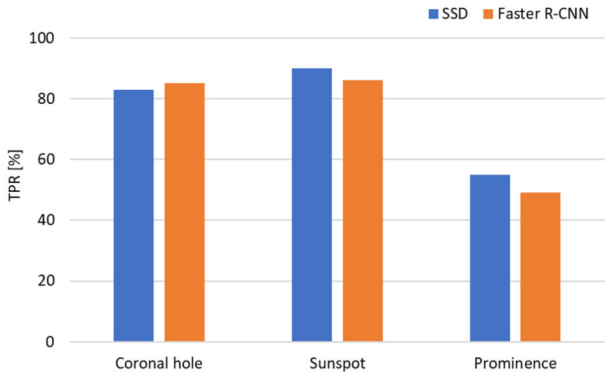

Figure 4 TPR scores of the trained models for different solar events.

using SSD and Faster R-CNN were relatively low at 59% and 52%, respectively. This indicates that the performance of classifying prominences using both models is significantly poor.

The TPR is a correctly identified fraction based on the total number of target objects in the training dataset. Figure 4 shows TPR results for each solar event. TPR scores for the coronal hole and sunspot detection were higher than that for prominence detection. The highest TPR score was recorded for sunspot detection: 90% using SSD and 86% using Faster R-CNN. For coronal hole detection, we obtained TPR scores of 83% and 85% using SSD and Faster R-CNN, respectively, which are similar. For prominence detection, we obtained lower TPR scores compared with the other solar events. Both models exhibit poor prominence detection and can detect approximately 50% of the labeled data.

In Figure 5, we display the bounding boxes of our dataset (left) and predicted boxes using SSD (center) and Faster R-CNN (right) for the same data to compare the prediction results of each model. The top panel is for coronal hole detection; the boxed area of Faster R-CNN looks similar to the bounding boxed area. The middle panel corresponds to sunspot detection, and the size of the detection boxes of the two models is similar to the bounding boxes. However, in some cases (e.g., the sunspot on the right of the solar disk), only one model can detect the sunspots. The bottom panel presents prominence detection, and only SSD can detect the prominences in some cases (e.g., the prominence on the bottom right of the solar limb).

We tested our trained SSD model, which had higher mAP than Faster R-CNN, with the HEK dataset. Figure 6 shows examples of the SSD test results using HEK. The top panel

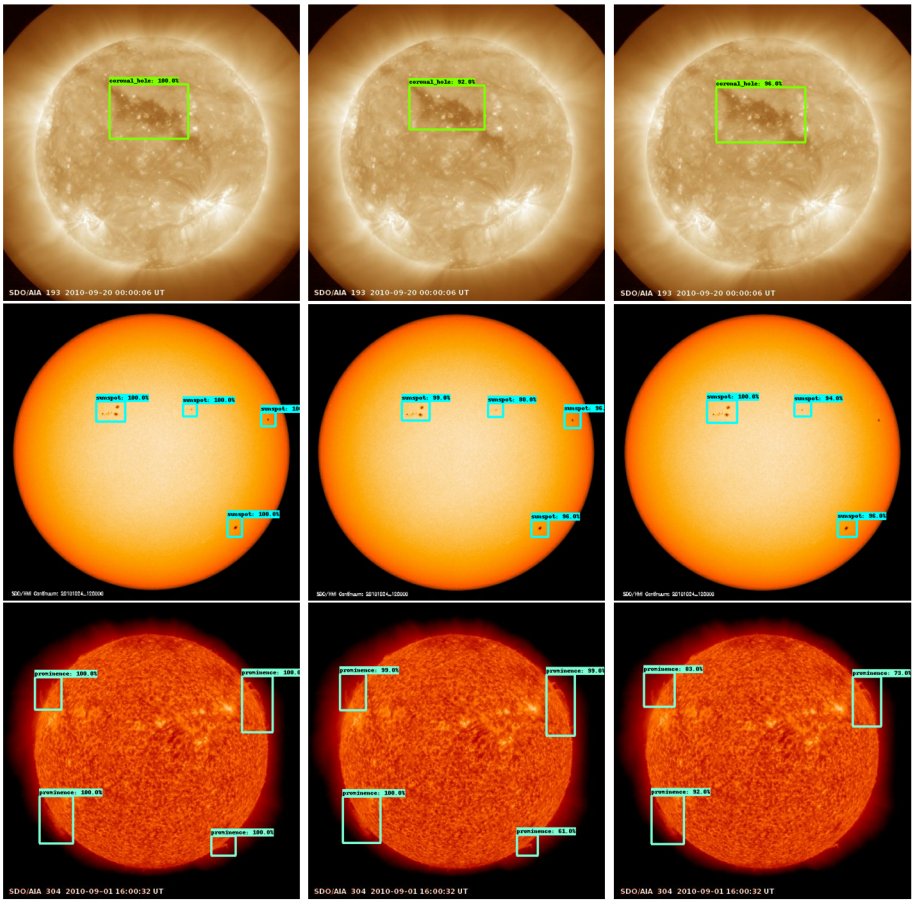

Figure 5 Sample bounding boxes of our dataset (left) and detection results for coronal hole (top), sunspots (middle), and prominences (bottom) using SSD (center) and Faster R-CNN (right) on the same dataset.

shows the prediction results from the SSD model and the bottom panel shows the bounding boxes of events from the HEK dataset. Our trained model found the coronal holes except the small size coronal holes in the HEK dataset which were out of the criteria of our dataset. In the case of sunspots, our trained model found sunspot groups that included small sunspots, whereas the HEK dataset detected smaller areas than the model prediction results which only included large sized sunspots. We visually extracted "areas of sunspots" since our sunspot dataset is aimed to extract the sunspot areas, not to distinguish the active regions. Therefore, the result of our model detected not only a sunspot but also sunspot groups that are relatively close to each other with a single box. In the case of prominences, our model detected off-limb prominences which are easily recognized by human eyes. Some events were missed in the HEK dataset because the HEK only recognized prominence events associated with filament structure which appeared on the solar disk. HEK is not designed for solar event detection only; hence, it did not serve the object detection purpose that we intended. As shown in Figure 6, our dataset was more appropriate as a label, and we recommend using our dataset when training deep-learning-based object-detection models.

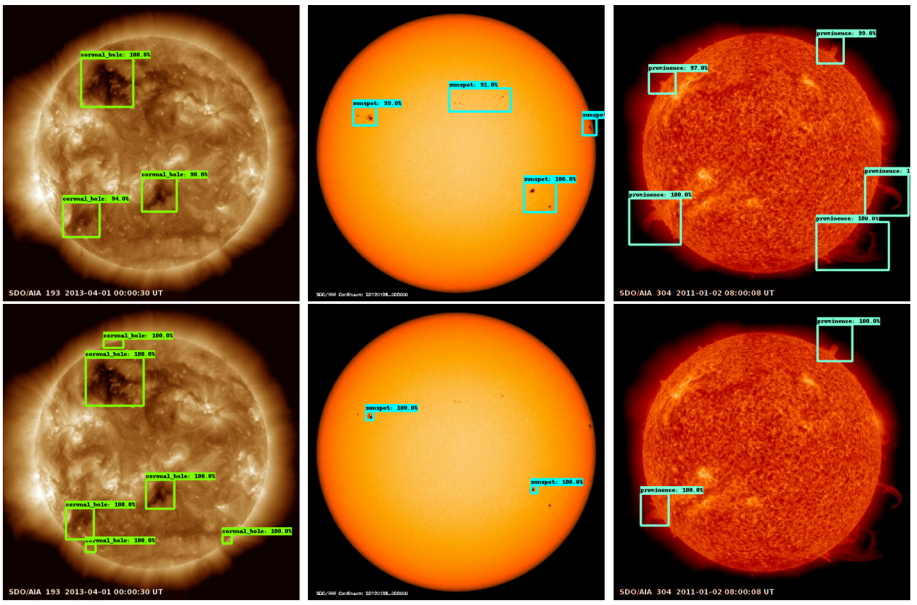

Figure 6 Examples of test results from our trained SSD model using HEK dataset. The top panel shows prediction results from SSD and the bottom panel shows bounding boxes of the events from HEK dataset. The left column corresponds to coronal holes, the central one to sunspots, and the right one to prominences.

5. Conclusion

We carried out a solar event detection investigation using two object detection methods: SSD and Faster R-CNN. We tested these models using coronal holes, sunspots, and prominences. Our results show that for solar event detection the performance of SSD is slightly higher than that of Faster R-CNN based on mAP. For sunspot detection, the AP of SSD exhibited a remarkable performance, reaching 99%. However, for coronal hole detection, Faster R-CNN is better than SSD, based on AP and the TPR score. The prominence detection performance of both models was relatively lower than that of other solar events. The overall performance of our results is high, due to the characteristics of the training data. Sunspots exhibit clear differences between the background and objects. Coronal holes have clearly defined characteristics in the data as well as a large area size. However, the performance of prominence detection is relatively low, which is also due to the nature of the data and events. Prominences have faint features compared with the other solar events types, and the complexity of the AIA 304 data influences the prediction of the region in the models. Additionally, Faster R-CNN performs better than SSD in coronal hole detection, owing to the method used to identify the bounding box. The region proposal network, which determines the bounding box in Faster R-CNN, tends to more accurately detect coronal holes, which are relatively large areas, by designating an area using multi-scale anchors.

Our study shows that using SSD and Faster R-CNN is a promising approach for solar event detection, and it provides excellent performance results for coronal hole and sunspot detection. Kucuk, Aydin, and Angryk (2017) detected solar events using Faster R-CNN and showed that the mAP (@0.5IoU) was 32% for coronal holes. Our results exhibited a significantly better performance – the mAP (@0.5IoU) of the coronal holes was 76%, and even

if the IoU threshold was increased to 0.7, the mAP (@0.7IoU) still exhibited good performance at 60%. We compared the object detection results of our dataset to the HEK dataset. Our dataset had sufficient accuracy to train deep learning models for object detection, which guarantees further achievements of object detection studies in solar physics. We believe that these object detection approaches can lead to more diverse solar event detection.

There are some limitations in our current work, which imply future directions for continued research. First, we plan to improve and expand our dataset. The bounding boxes for small sunspots can be more precise and distinguished from large sunspot groups. In addition, other solar event types such as filaments, flares, and coronal loops will be included. Then, we will examine the performance of these models on other solar event types. We intend to use Hα image data to detect filaments because they are more clearly visible in these images. In the case of flares, a method to determine the entire duration of the flaring time will be studied. We will also investigate other deep learning models for solar event detection. In particular, we expect that the application of instance segmentation algorithms, such as Mask R-CNN, to sunspot and coronal hole detection will provide fine detection of the area and estimate a more accurate size. Moreover, we intend to publish a solar event catalog including the coordinates and other parameters of the detected events.

Acknowledgements The SDO data were provided by the Korean Data Center (KDC) for SDO in cooperation with NASA, Stanford University (JSOC), and KISTI (KREONET), which is supported by the "Next Generation Space Weather Observation Network" project of the Korea Astronomy and Space Science Institute (KASI). This work was also supported by the Institute for Information and Communications Technology Planning and Evaluation (IITP) grant funded by the Korea government (MSIT) (No. 2019-0-01343, Training Key Talents in Industrial Convergence Security)

Declarations

Disclosure of Potential Conflicts of Interest The authors declare that there are no conflicts of interest.

References

Armstrong, J.A., Fletcher, L.: 2019, Fast solar image classification using deep learning and its importance for automation in solar physics. *Solar Phys.* **294**, 80.

Aschwanden, M.J.: 2010, Image processing techniques and feature recognition in solar physics. *Solar Phys.* **262**, 235.

Aschwanden, M.J., Lee, J.K., Gary, G.A., Smith, M., Inhester, B.: 2008, Extraction of solar coronal magnetic loops with the directional 2D Morlet wavelet transform. *Solar Phys.* **248**, 359.

Banda, J.M., Angryk, R.A.: 2010, Selection of image parameters as the first step towards creating a CBIR system for the Solar Dynamics Observatory. In: *Proc. Int. Conf. on Digital Image Computing: Techniques and Applications*, 528.

Banda, J.M., Angryk, R.A.: 2014, Large-scale region-based multimedia retrieval for solar images. In: *Proc. Int. Conf. on Artificial Intelligence and Soft Computing*, *Zakopane, Poland*, 649.

Brajša, R., Sudar, D., Benz, A.O., Skokić, I., Bárta, M., Pontieu, B.D., Kim, S., Kobelski, A., Kuhar, M., Shimojo, M., Wedemeyer, S., White, S., Yagoubov, P., Yan, Y.: 2018, First analysis of solar structures in 1.21 mm full-disc ALMA image of the Sun. *Astron. Astrophys.* **613**, A17.

Cai, Z., Vasconcelos, N.: 2018, Cascade R-CNN: delving into high quality object detection. In: *Proc. IEEE/CVF Conf. on Computer Vision and Pattern Recognition*.

Curto, J.J., Blanca, M., Martinez, E.: 2008, Automatic sunspots detection on full-disk solar images using mathematical morphology. *Solar Phys.* **250**, 411.

Dai, J., Li, Y., He, K., Sun, J.: 2016, R-FCN: object detection via region-based fully convolutional networks. In: *Proc. 30th Conf. on Neural Information Processing Systems*, *NIPS 2016*, 1.

Girshick, R.: 2015, Fast R-CNN. In: *Proc. IEEE Int. Conf. on Computer Vision*, 1440.

Girshick, R., Donahue, J., Darrell, T., Malik, J.: 2014, Rich feature hierarchies for accurate object detection and semantic segmentation. In: *Proc. IEEE Conf. on Computer Vision and Pattern Recognition*, *CVPR*, 1.

He, K., Zhang, X., Ren, S., Sun, J.: 2016, Deep residual learning for image recognition. In: *Proc. IEEE Conf. on Computer Vision and Pattern Recognition*, *CVPR*, 770.

He, K., Gkioxari, G., Dollár, P., Girshick, R.: 2017, Mask R-CNN. In: *Proc. IEEE Int. Conf. on Computer Vision*, *ICCV*, 2380.

Huang, J., Rathod, V., Sun, C., Zhu, M., Korattikara, A., Fathi, A., Fischer, I., Wojna, Z., Song, Y., Guadarrama, S., Murphy, K.: 2017, Speed/accuracy trade-offs for modern convolutional object detectors. In: *Proc. IEEE Conf. on Computer Vision and Pattern Recognition*, *CVPR*, 3296.

Hurlburt, N., Cheung, M., Schrijver, C., Chhang, L., Freeland, S., Green, S., Heck, C., Jaffey, A., Kobashi, A., Schiff, D., Serafin, J., Seguin, R., Slater, G., Somani, A., Timmons, R.: 2012, Heliophysics event knowledgebase for the Solar Dynamics Observatory (SDO) and beyond. *Solar Phys.* **275**, 67.

Inhester, B., Feng, L., Wiegelmann, T.: 2008, Segmentation of loops from coronal EUV images. *Solar Phys.* **248**, 379.

Ireland, J., Young, C.A., McAteer, R.T.J., Whelan, C., Hewett, R.J., Gallagher, P.T.: 2008, Multiresolution analysis of active region magnetic structure and its correlation with the Mount Wilson classification and flaring activity. *Solar Phys.* **252**, 121.

Jeong, H.-J., Moon, Y.J., Park, E., Lee, H.: 2020, Solar coronal magnetic field extrapolation from synchronic data with AI-generated farside. *Astrophys. J.* **903**, L25.

Kim, S., Park, J.-Y., Kim, Y.-H.: 2017, Solar cycle variation of microwave polar brightening and EUV coronal hole observed by Nobeyama Radioheliograph and SDO/AIA. *J. Korean Astron. Soc.* **50**, 125.

Kim, T., Park, E., Lee, H., Moon, Y.-J., Bae, S.-H., Lim, D., Jang, S., Kim, L., Cho, I.-H., Choi, M., Cho, K.-S.: 2019, Solar farside magnetograms from deep learning analysis of STEREO/EUVI data. *Nature Astron.* **3**, 397.

Kucuk, A., Aydin, B., Angryk, R.: 2017, Multi-wavelength solar event detection using faster R-CNN. In: *Proc. IEEE Int. Conf. on Big Data*, 2552.

Kucuk, A., Banda, J.M., Angryk, R.A.: 2017, Solar event classification using deep convolutional neural networks. In: *Proc. Int. Conf. on Artificial Intelligence and Soft Computing*, 118.

Lee, J.K., Newmann, T.S., Gary, G.A.: 2006, Oriented connectivity-based method for segmenting solar loops. *Pattern Recognit.* **39**, 246.

Lemen, J.R., Title, A.M., Akin, D.J., Boerner, P.F., Chou, C., Drake, J.F., Duncan, D.W., Edwards, C.G., Friedlaender, F.M., Heyman, G.F., Hurlburt, N.E., Katz, N.L., Kushner, G.D., Levay, M., Lindgren, R.W., Mathur, D.P., McFeaters, E.L., Mitchell, S., Rehse, R.A., Schrijver, C.J., Springer, L.A., Stern, R.A., Tarbell, T.D., Wuelser, J.-P., Wolfson, C.J., Yanari, C., Bookbinder, J.A., Cheimets, P.N., Caldwell, D., Deluca, E.E., Gates, R., Golub, L., Park, S., Podgorski, W.A., Bush, R.I., Scherrer, P.H., Gummin, M.A., Smith, P., Auker, G., Jerram, P., Pool, P., Soufli, R., Windt, D.L., Beardsley, S., Clapp, M., Lang, J., Waltham, N.: 2012, The Atmospheric Imaging Assembly (AIA) on the Solar Dynamics Observatory (SDO). *Solar Phys.* **275**, 17.

Lin, T.-Y., Goyal, P., Girshick, R., He, K., Dollar, P.: 2017, Focal loss for dense object detection. In: *Proc. IEEE Int. Conf. on Computer Vision*, *ICCV*, 2980.

Liu, W., Anguelov, D., Erhan, D., Szegedy, C., Reed, S., Fu, C.-Y., Berg, A.C.: 2016, SSD: single shot multibox detector. In: *Proc. European Conf. on Computer Vision*, *ECCV*, 21.

Martens, P., Attrill, G., Davey, A., Engell, A., Farid, S., Grigis, P., Kasper, J., Korreck, K., Saar, S., Savcheva, A., Su, Y., Testa, P., Wills-Davey, M., Bernasconi, P.N., Raouafi, N.-E., Delouille, V.A., Hochedez, J.F., Cirtain, J.W., DeForest, C.E., Angryk, R.A., Moortel, I.D., Wiegelmann, T., Georgoulis, M.K., McAteer, R.T.J., Timmons, R.P.: 2012, Computer vision for the Solar Dynamics Observatory (SDO). *Solar Phys.* **275**, 79.

McAteer, R.T.J., Gallagher, P.T., Ireland, J., Young, C.A.: 2005, Automated boundary-extraction and region-growing techniques applied to solar magnetograms. *Solar Phys.* **228**, 55.

Park, E., Moon, Y.-J., Shin, S., Yi, K., Lim, D., Lee, H., Shin, G.: 2018, Application of the deep convolutional neural network to the forecast of solar flare occurrence using full-disk solar magnetograms. *Astrophys. J.* **869**, 91.

Park, E., Moon, Y.-J., Lim, D., Lee, H.: 2020, De-noising SDO/HMI solar magnetograms by image translation method based on deep learning. *Astrophys. J.* **891**, L4.

Portier-Fozzani, F., Vandame, B., Bijaoui, A., Maucherat, A.J., Team, E.: 2001, A Multiscale Vision Model applied to analyze EIT images of the solar corona. *Solar Phys.* **201**, 271.

Priest, E.: 2014, *Magnetohydrodynamics of the Sun*, Cambridge University Press, Cambridge. DOI. ISBN: 9781139020732.

Rahman, S., Moon, Y.-J., Park, E., Siddique, A., Cho, I.-H., Lim, D.: 2020, Super-resolution of SDO/HMI magnetograms using novel deep learning methods. *Astrophys. J.* **897**, L32.

Redmon, J., Divval, S., Girshick, R., Farhadi, A.: 2016, You only look once: unified, real-time object detection. In: *Proc. IEEE Conf. on Computer Vision and Pattern Recognition*, *CVPR*, 779.

Ren, S., He, K., Girshick, R., Sun, J.: 2017, Faster R-CNN: towards real-time object detection with region proposal networks. *IEEE Trans. Pattern Anal. Mach. Intell.* **39**, 6.

Scherrer, P.H., Schou, J., Bush, R.I., Kosovichev, A.G., Bogart, R.S., Hoeksema, J.T., Liu, Y., Duvall Jr., T.L., Zhao, J., Title, A.M., Schrijver, C.J., Tarbell, T.D., Tomczyk, S.: 2012, The Helioseismic and Magnetic Imager (HMi) investigation for the Solar Dynamics Observatory (SDO). *Solar Phys.* **275**, 207.

Schou, J., Scherrer, P.H., Bush, R.I., Wachter, R., Couvidat, S., Rabello-Soares, M.C., Bogart, R.S., Hoeksema, J.T., Liu, Y., Duvall Jr., T.L., Akin, D.J., Allard, B.A., Miles, J.W., Rairden, R., Shine, R.A., Tarbell, T.D., Title, A.M., Wolfson, C.J., Elmore, D.F., Norton, A.A., Tomczyk, S.: 2012, Design and ground calibration of the Helioseismic and Magnetic Imager (HMI) instrument on the Solar Dynamics Observatory (SDO). *Solar Phys.* **275**, 229.

Tzutalin: 2015, *LabelImg git code*. https://github.com/tzutalin/labelImg.

Woods, T.N., Eparvier, F.G., Hock, R., Jones, A.R., Woodraska, D., Judge, D., Didkovsky, L., Lean, J., Mariska, J., Warren, H., McMullin, D., Chamberlin, P., Berthiaume, G., Bailey, S., Fuller-Rowell, T., Sojka, J., Tobiska, W.K., Viereck, R.: 2012, Extreme Ultraviolet Variability Experiment (eve) on the Solar Dynamics Observatory (SDO): overview of science objectives, instrument design, data products, and model developments. *Solar Phys.* **275**, 115.

Zhang, S., Wen, L., Bian, X., Lei, Z., Li, S.Z.: 2018, Single-shot refinement neural network for object detection. In: *Proc. IEEE Conf. on Computer Vision and Pattern Recognition*, *CVPR*, 4203.